How to cite: *Angew. Chem. Int. Ed.* **2022,** *61,* e202205018
International Edition: doi.org/10.1002/anie.202205018
German Edition: doi.org/10.1002/ange.202205018

Fused-Ring Systems

Doubling the Length of the Longest Pyrene-Pyrazinoquinoxaline Molecular Nanoribbons

*Félix Hernández-Culebras, Manuel Melle-Franco, and Aurelio Mateo-Alonso**

Dedicated to the memory of Professor John S. Fossey

Abstract: Molecular nanoribbons are a class of atomically-precise nanomaterials for a broad range of applications. An iterative approach that allows doubling the length of the longest pyrene-pyrazinoquinoxaline molecular nanoribbons is described. The largest nanoribbon obtained through this approach—with a 60 linearly-fused ring backbone (14.9 nm) and a 324-atoms core ($C_{276}N_{48}$)—shows an extremely high molar absorptivity (values up to 1 198 074 $M^{-1}cm^{-1}$) that also endows it with a high molar fluorescence brightness (8700 $M^{-1}cm^{-1}$).

Graphene nanoribbons (NRs)—nanographenes that extend in one-dimension—have shown much promise in a broad range of electronic, photonic and spintronic applications.[1] The electronic, optical and magnetic properties of NRs depend on a series of structural variables such as edge structure, width, length and heteroatom doping. For this reason, the synthesis of NRs with atomic precision is key to establish their fundamental properties, validate theoretical predictions, and also to target the specific properties required by different applications.

Organic synthesis has recently emerged among the different top-down[1a,2] and bottom-up[1a–k,2,3] approaches to prepare NRs. This is because, it can provide control over all the structural variables that dominate the properties of NRs. The synthesis of different families of increasingly longer molecular NRs[1c,d,f,3b,4] has revealed how some of their properties can be influenced by the length. In particular, increasing molar absorptivities have been observed with increasing NR lengths. For instance, the longest molecular NR with a 53 linearly-fused rings backbone of 12.9 nm[4t] has shown record molar absorptivities as high as 986 100 $M^{-1}cm^{-1}$. Such high molar absorptivities are highly desirable for photovoltaic and photodetector applications,[5] but also endow fluorescent nanomaterials with an enhanced brightness for biomedical and energy applications.[6] Yet, despite the remarkable advances, the synthesis of longer molecular NR remains challenging, as their synthetic routes require an increasing number of synthetic and purification steps that need to be optimized individually.

In 2018, we reported the first iterative approach for the synthesis of molecular NRs, which was aimed at simplifying their synthesis.[4k] This approach consists on the consecutive assembly of building block **A** into a NR by repeating the same set of reactions that allows incorporating 10-ring-long segments per iteration (Figure 1a). Through this approach, we were able to synthesise **NR-30**[4k]—with a 30 linearly-fused rings backbone of 7.7 nm—after three iterations. **NR-30** remains to this date the largest pyrene-pyrazinoquinoxaline NR. Even if, it should be possible to obtain longer NRs by increasing the number of iterations, we found it difficult

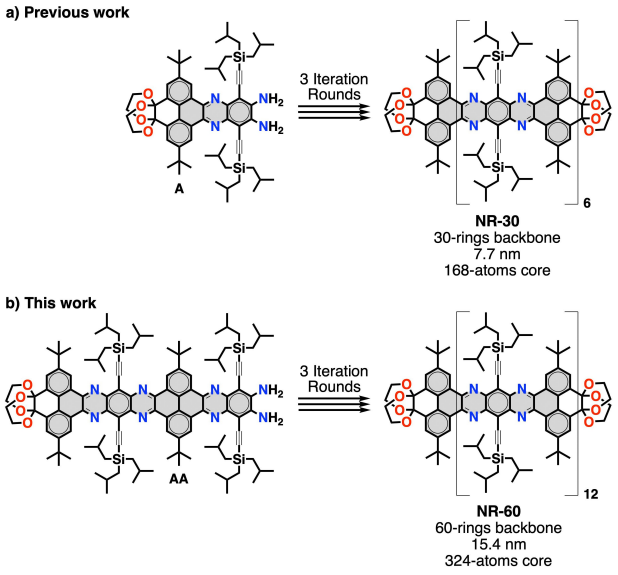

Figure 1. Iterative synthetic methods of pyrene-pyrazinoquinoxaline molecular NRs.

[*] F. Hernández-Culebras, Prof. Dr. A. Mateo-Alonso
POLYMAT, University of the Basque Country UPV/EHU
Avenida de Tolosa 72, 20018 Donostia-San Sebastián (Spain)
E-mail: amateo@polymat.eu
M. Melle-Franco
CICECO—Aveiro Institute of Materials, Department of Chemistry, University of Aveiro
3810–193 Aveiro (Portugal)
Prof. Dr. A. Mateo-Alonso
Ikerbasque, Basque Foundation for Science
48009 Bilbao (Spain)

to run more than three iterations, because of the challenging purification of this type of NRs that led to reduced isolated yields after each iteration.

Herein, we describe an iterative methodology that allows doubling the length of the longest pyrene-pyrazinoquinoxaline molecular NRs. This methodology relies on the introduction of a new building block (**AA**) with an aromatic backbone that doubles the length of its predecessor (Figure 1b). Consequently, by running iteration rounds with building block **AA**, 20-ring-long segments are incorporated into the NR per iteration. As such, a series of pyrene-pyrazinoquinoxaline molecular NRs (**NR-20**, **NR-40** and **NR-60**) with a 20-, 40- and 60-ring backbone has been achieved after one, two, and three iteration rounds, respectively (Scheme 1). The length of **NR-40** (10.1 nm) already surpasses the current length record for pyrene-pyrazinoquinoxaline NRs. Whereas, the length of **NR-60** (14.9 nm) does not only double the current length record for pyrene-pyrazinoquinoxaline NRs, but also sets a new record as the longest molecular NR. Remarkably, **NR-40** and **NR-60** also show a high solubility in common organic solvents at room temperature, which allows establishing their structure and fundamental properties by a broad range of structural, optoelectronic and redox characterization techniques. This new family of NRs show extremely high molar absorptivity values that increase with the length reaching, in the case of **NR-60**, up to 1 198 074 $M^{-1}cm^{-1}$ that surpass those observed in the largest molecular NRs and in single-chromophore nanographenes. Furthermore, the high molar absorptivity endows **NR-60** with a high molar brightness of 8700 $M^{-1}cm^{-1}$.

Building block **AA** comprises a tetrabenzobenzohexaazanonacene core equipped with *o*-diamines at one end, and diacetal-protected *o*-dione functionalities at the other end (Scheme 1). *o*-Diamines and *o*-diones have been selected as they converge through the formation of a pyrazine ring by an imine-type cyclocondensation reaction, which provide an efficient mean to interconnect building blocks. The *o*-dione functionalities have been protected to avoid the self-condensation of building block **AA**, and thus, enable the controlled condensation of one building block after the other. *tert*-Butyl and tri-*iso*-butylsilyl solubilizing groups were used because of their relatively small size and large solubilising power.[4k] The synthesis of building block **AA** was achieved following the route set out in Scheme 2. Compound **A** was obtained in 12 steps using a procedure previously described by some of us,[4k] whereas compound **C** was obtained in 6 steps (details in the Supporting Information). Condensation between the free amines of compound **A** and the free diones of compound **C** yielded thiadiazolotetrabenzohexaazanonacene **D** (96 %), which was subsequently reduced in the presence of $LiAlH_4$ into **AA** (quantitative).

The cyclocondensation of 2.5 equivalents of **AA** with 2,7-di-*tert*-butylpyrene-4,5,9,10-tetraone **B**[7] gave **NR-20** in a 67 % yield after chromatographic purification (Scheme 1). Then, the terminal diones of **NR-20** were deprotected in the presence of TFA/H_2O and the crude was subsequently cyclocondensed with 2.5 equivalents of **AA** to give **NR-40** in a 22 % yield over the two steps after purification by preparative gel permeation chromatography. The same deprotection/condensation process was repeated on **NR-40** by deprotecting the terminal diones in TFA/H_2O that were subsequently cyclocondensed in the presence of 5 equivalents of **AA** to provide **NR-60** in a 26 % yield over the two steps after purification by preparative gel permeation chromatography. **NR-20**, **NR-40** and **NR-60** are soluble in common chlorinated solvents, such as $CHCl_3$, CH_2Cl_2 and *o*-dichlorobenzene (ODCB).

The structure of the NRs was confirmed by ^1H and ^{13}C NMR at room temperature in $CDCl_3$ (Figure 2 and Supporting Information). The structural (and also optoelectronic and redox) data of **NR-20** prepared from **AA** is identical as that of **NR-20** prepared from **A**.[4k] The NMR signals in the aromatic and aliphatic region are consistent with the structure and most importantly with the molecular weights of the different NRs. For instance, the integration in the ^1H NMR spectra can be used to establish unambiguously the length of the NR, as signal of the inner pyrene protons *a* (the assignments correspond to the lettering shown in Scheme 1) integrates 12, 28 and 44 protons, respectively for **NR-20**, **NR-40** and **NR-60**, whereas the signals of the protons *b*, *c*, and *d* at the terminal pyrene show a constant integration of 4, 4 and 16 in all NRs independently of the length of the NR (Figure 2). Matrix-assisted laser desorption/ionization time of flight mass spectrometry (MALDI-TOF MS) show the expected molecular ion peaks for **NR-20** and **NR-40**. In the case of **NR-60**, while the structure has been confirmed unambiguously by NMR, we have not been able to detect the molecular ion peak. Similar observations have been reported for another type of high molecular weight pyrene NRs.[8]

When dissolved, **NR-20**, **NR-40** and **NR-60** give rise to fuchsia solutions similar to the colour of the solids (inset Figure 3a). The electronic absorption features of the NR series in chloroform are consistent with their structure and with previous observations on other members of this pyrene-pyrazinoquinoxaline NR family (Table S1),[4k] which further support the structural assignments. The electronic absorption spectra show a small band at 605 nm, a set of bands with clear vibronic features in-between 400–600 nm and another set in the UV region, which were assigned to the α, ρ, and β bands[9] from longer to shorter wavelengths, respectively (Figure 3a and Table S2). The wavelength of the α band (with maxima at 604 nm in all cases) is independent of the length of the NR, while the ρ (with maxima at 545, 550 and 553 nm, respectively for **NR-20**, **NR-40** and **NR-60**) and the β bands (with maxima at 383, 385 and 387 nm, respectively for **NR-20**, **NR-40** and **NR-60**) show a clear bathochromic shift with increasing lengths. Remarkably, the molar attenuation coefficients of **NR-20** ($\varepsilon^{\beta} = 425\,358\ L\,mol^{-1}cm^{-1}$), **NR-40** ($\varepsilon^{\beta} = 789\,164\ L\,mol^{-1}cm^{-1}$), and **NR-60** ($\varepsilon^{\beta} = 1\,198\,074\ L\,mol^{-1}cm^{-1}$) increase with increasing lengths as an effect of the more extended π-system. The maximum molar attenuation coefficient value for **NR-60** surpasses the largest values reported for giant nanographene chromophores (986 100 $M^{-1}cm^{-1}$ for $C_{296}N_{24}S_2$;[4t] 844 000 $M^{-1}cm^{-1}$ for C_{186}[10]). The experimental HOMO–

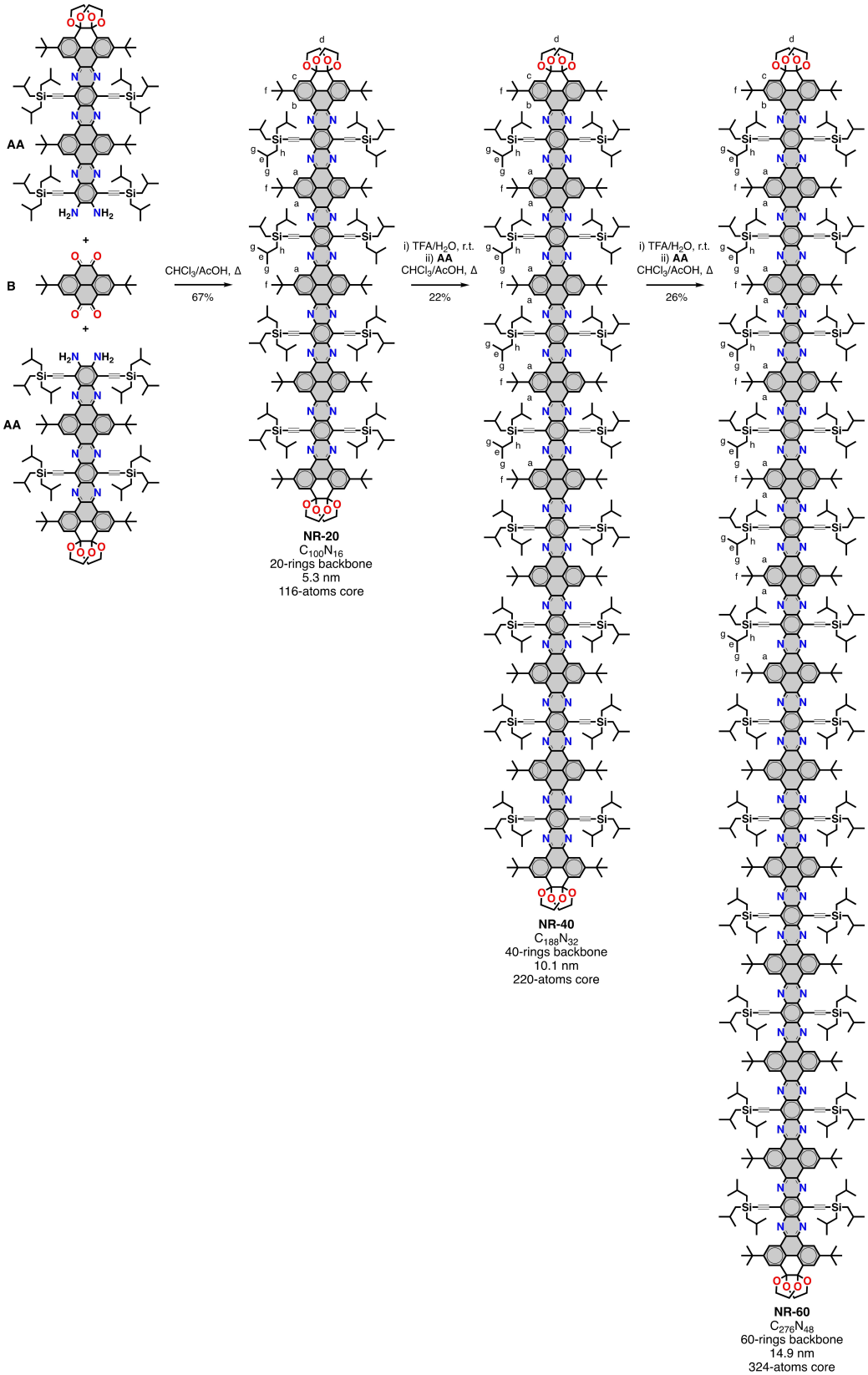

Scheme 1. Iterative synthesis of **NR-20**, **NR-40** and **NR-60**. The lettering indicates the proton assignments on the ^{1}H NMR spectra and in the Supporting Information. The molecular formula indicates only the atoms in the aromatic core (highlighted in grey).

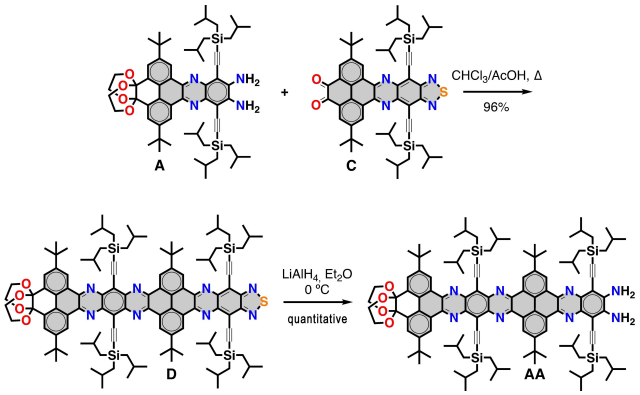

Scheme 2. Synthetic route for building block **AA**. Complete details are given in the Supporting Information.

LUMO gap (E_{gap}) values were estimated from the onset of the longest wavelength transition. The E_{gap} values of **NR-20** (1.96 eV), **NR-40** (1.96 eV) and **NR-60** (1.96 eV) are the same, independently of the length of the NR. This is consistent with previous observations that show how the E_{gap} values of pyrene-quinoxaline NRs decrease rapidly for NRs with a backbone from 6 to 10 linearly-fused rings ($E_{gap}^{6\text{-rings}} = 2.80$ eV,[11] $E_{gap}^{8\text{-rings}} = 2.40$ eV,[11] and $E_{gap}^{10\text{-rings}} = 1.97$ eV[4k]) and then for backbones >10 rings the E_{gap} values saturate and remains almost invariable.[4k] This trend is consistent with that observed on other types of narrow NRs.[4t,12]

In contrast to most soluble giant nanographenes, which generally show weak or no fluorescence,[13] solutions of **NR-20**, **NR-40** and **NR-60** show a bright magenta fluorescence upon exposure to UV light (inset Figure 3b). The fluorescence spectra of **NR-20**, **NR-40** and **NR-60** in chloroform are almost superimposable and show a vibronically-resolved fluorescence band (with maxima at 623, 623 and 625 nm, respectively) that span from 600 to 800 nm (Figure 3b and Table S2). This is in agreement with the florescence spectra reported for pyrene-pyrazinoquinoxaline

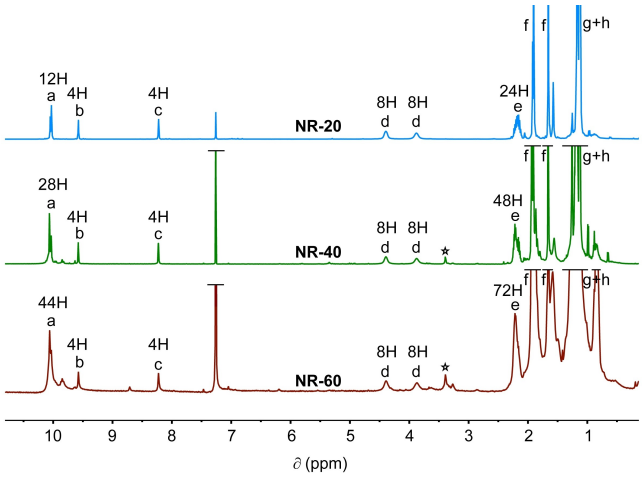

Figure 2. ^{1}H NMR spectra of **NR-20**, **NR-40** and **NR-60** in $CDCl_3$ at room temperature. Stars designate solvent residual peaks.

NRs with >10-ring backbones[4k] that also show the same fluorescence band as it emerges from the α absorption band that remains at the same energy independently of the length (Table S1). The fluorescence quantum yields (Φ) of **NR-20**, **NR-40** and **NR-60** show values of 0.18, 0.16 and 0.11, respectively, which are remarkable considering the size of their aromatic core. These quantum yield values are comparable to those of current state-of-the-art carbon quantum dots in the same spectral region.[6a,14] Considering their high molar absorption, the molar fluorescence brightness ($\varepsilon\Phi$) and mass fluorescence brightness values (($\varepsilon\Phi$)/molecular weight) of **NR-20** ($5534\ M^{-1}cm^{-1}$ and $1.3\ g^{-1}Lcm^{-1}$, respectively), **NR-40** ($9950\ M^{-1}cm^{-1}$ and $1.3\ g^{-1}Lcm^{-1}$, respectively) and **NR-60** ($8700\ M^{-1}cm^{-1}$ and $0.8\ g^{-1}Lcm^{-1}$, respectively) surpass those reported for carbon quantum dots ($\approx 4000\ M^{-1}cm^{-1}$ and $\approx 0.2\ g^{-1}Lcm^{-1}$, respectively).[6b,c]

The redox properties of **NR-20**, **NR-40** and **NR-60** were studied by cyclic voltammetry. All the three NRs exhibited three waves on the cathodic side that overlap in some cases (Figure 3c and Table S2) and that are consistent with the structure and with previous reports on shorter pyrene-pyrazinoquinoxaline NRs (Table S1).[4k] The first reduction half-wave potentials ($E_{1/2}$) of the NRs were very similar ($E_{1/2}^{NR\text{-}20} = -1.14$ V, $E_{1/2}^{NR\text{-}40} = -1.16$ V, $E_{1/2}^{NR\text{-}60} = -1.05$ V vs Fc/Fc^+) and confirm that all the NRs are electron-deficient materials. The electrochemical LUMO or electron affinities (E_{LUMO}) were estimated from the onset potential of the first reduction wave of the cyclic voltammograms. The E_{LUMO} values (−3.62, −3.72 and −3.74 eV, respectively for **NR-20**, **NR-40** and **NR-60**) are very similar and tend to decrease with the increasing the size of the NR's backbone.

We have not been able to obtain crystals suitable for X-ray diffraction, so we relied on calculations (B3LYP-6-31G(d,p)) to get an insight into the structure of the NRs. Calculations were carried out on **NR-20-H**, **NR-40-H** and **NR-60-H**, in which the *tert*-butyl and tri-*iso*-butylsilyl solubilizing groups have been substituted by hydrogen atoms for computational efficiency. The models of **NR-20-H**, **NR-40-H** and **NR-60-H** illustrate a virtually flat backbone with lengths of 5.3, 10.1 and 14.9 nm, respectively. The dominant resonance structure in all the NRs is best represented by Clar structures (as shown in Scheme 1) with a biphenyl group (2 sextets) in the pyrene residues, and an anthracene group (1 sextet) in the pyrazinoquinoxaline residues. This is consistent with bond-length alternation analysis (Figures 3d and S1) that show nearly aromatic distances on the off-linear pyrene rings and on the pyrazinoquinoxaline residues, whereas distances that approximate to single bonds are observed on the pyrene rings on the linear backbone. This is also consistent with the negative NICS(0) values (Figures 3d and S1) found on almost all the off-linear rings of the pyrene and of the pyrazinoquinoxaline residues (shown in red), whereas positive values (shown in blue) were observed on the pyrene rings on the linear backbone. The anisotropy of the induced current density (ACID) plots of **NR-20**, **NR-40** and **NR-60** (Figures 3e and S2) are also consistent with this assignment and shows a diamagnetic current that goes

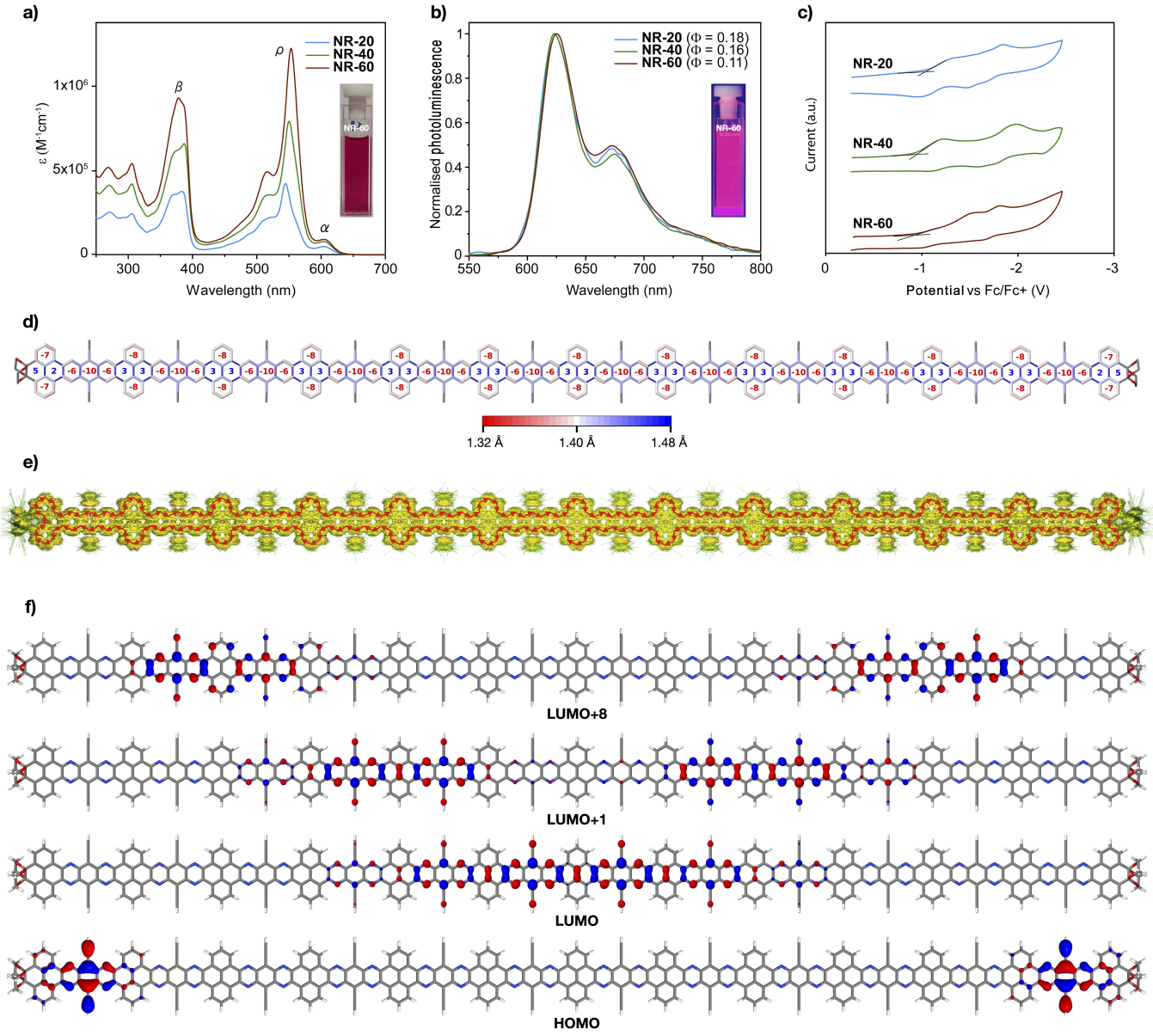

Figure 3. a) Absorption and b) fluorescence (λ_{ex} = 415 nm) spectra in $CHCl_3$ (insets show a solution of **NR-60** under natural and UV light, respectively) and c) cyclic voltammograms in *n*-Bu_4NPF_6/ODCB (20 mV s^{-1}) of **NR-20**, **NR-40**, and **NR-60**. d) Bond length analysis and NICS(0) values of **NR-60-H**. Bonds are rendered in a color continuum ranging from red (1.31 A) to white (1.40 A) to blue (1.49 A) so that Clar's aromatic sextets are lighter/whiter colors and localized double and single bonds are red and blue, respectively. e) ACID plots of **NR-60-H**. f) Representative B3LYP-6-31G(d,p) frontier orbitals for **NR-60**.

around the NR periphery (red trace) and that has been described for other types of NRs.[4t,15]

To shine additional light on the optoelectronic and redox properties, we carried out DFT calculations (B3LYP-6-311 + g(2d,p)-Chloroform/B3LYP-6-31G(d,p)) that reveal a set of quasidegenerate HOMO orbitals and a set of quasidegenerate LUMO orbitals in all NRs (Table S3). The near degeneracy increases with increasing lengths (4, 8 and 12 quasidegenerate HOMO orbitals and 4, 8 and 12 quasidegenerate LUMO orbitals, respectively for **NR-20-H**, **NR-40-H** and **NR-60-H**). The computed E_{gap} values (2.26, 2.23, and 2.22 eV, respectively for **NR-20-H**, **NR-40-H** and **NR-60-H**) and E_{LUMO} values (−3.32, −3.36, −3.37 eV, respectively for **NR-20-H**, **NR-40-H** and **NR-60-H**) correlate very well with the experimental ones and also show the same trend. The quasidegenerate HOMOs and LUMOs show electron densities mostly localised in specific segments of the different NR (Figures S3–S5), which in some cases can spread over as many as 28 consecutive rings along the linear backbone (representative HOMO, LUMO, LUMO + 1 and LUMO + 8 of **NR-60** are shown in Figure 3f). TD-DFT reveals that the α band of the electronic absorption spectra corresponds in all cases to the transitions between the HOMO-1/HOMO and all the quasidegenerate LUMO orbitals (Table S4). Whereas the ρ band shows a major contribution from the lowest quasidegenerate HOMO (HOMO-4, HOMO-8 and

HOMO-12, respectively for **NR-20-H**, **NR-40-H** and **NR-60-H**) and the LUMO (Table S4). The energies of the computed absorption bands (Figure S6 and Table S4) show the same trends observed experimentally, where the energy of the α band is independent of the length and the energy ρ band decrease with increasing lengths.

Overall, we have reported a new iterative synthetic approach that allow preparing molecular NRs with lengths that double the current length record of the pyrene-pyrazinoquinoxaline family and also sets a new length record as the longest molecular NR. The synthesis relies on the iterative coupling of a double sized building block that allows to double the length of the resulting NRs after each iterative round. The NRs are soluble in common organic solvents at room temperature, which made possible their purification and also their structural, optoelectronic and redox characterization in solution. Optoelectronic characterization evidence the remarkable light absorbing capabilities of the NRs that increase with the length of the backbone. In the case of **NR-60**, the molar absorptivities (up to 1 198 074 $L\,mol^{-1}\,cm^{-1}$) surpass the largest values reported for other giant nanographene chromophores[4t,10] and endows it with a high fluorescence brightness (8700 $M^{-1}\,cm^{-1}$). Overall, this work provides a new approach for the synthesis of giant molecular NRs with remarkable optoelectronic properties that derive form their large dimensions. This work also paves the way for the synthesis of other types of giant NRs and nanographenes that may find applications in sensing, energy and biomedicine.

Acknowledgements

This work was carried out with support from the Basque Science Foundation for Science (Ikerbasque), POLYMAT, the University of the Basque Country, Diputación de Guipúzcoa, Gobierno Vasco (BERC programme) and Gobierno de España (Project CEX2020-001067-M financed by MCIN/AEI/10.13039/501100011033). Technical and human support provided by SGIker of UPV/EHU and European funding (ERDF and ESF) is acknowledged. This project has received funding from the European Research Council (ERC) under the European Union's Horizon 2020 research and innovation programme (Grant Agreement No. 722951). This project has received funding from the European Union's Horizon 2020 research and innovation programme under grant agreement No. 899895. In addition, support through the project IF/00894/2015, the advanced computing project CPCA/A2/2524/2020 granting access to the Navigator cluster at LCA-UC and within the scope of the project CICECO-Aveiro Institute of Materials, UIDB/50011/2020 & UIDP/50011/2020 funded by national funds through the Portuguese Foundation for Science and Technology I.P./MCTES is gratefully acknowledged.

Conflict of Interest

The authors declare no conflict of interest.

Data Availability Statement

The data that support the findings of this study are available in the Supporting Information of this article.

Keywords: Giant Aromatics · Graphene Nanoribbons · Molecular Nanoribbons · Nanographenes · Polycyclic Aromatic Hydrocarbons

[1] a) L. Chen, Y. Hernandez, X. Feng, K. Müllen, *Angew. Chem. Int. Ed.* **2012**, *51*, 7640–7654; *Angew. Chem.* **2012**, *124*, 7758–7773; b) Y. Yano, N. Mitoma, H. Ito, K. Itami, *J. Org. Chem.* **2020**, *85*, 4–33; c) A. Mateo-Alonso, *Chem. Soc. Rev.* **2014**, *43*, 6311–6324; d) Z. Cai, M. A. Awais, N. Zhang, L. Yu, *Chem* **2018**, *4*, 2538–2570; e) A. Jolly, D. Miao, M. Daigle, J.-F. Morin, *Angew. Chem. Int. Ed.* **2020**, *59*, 4624–4633; *Angew. Chem.* **2020**, *132*, 4652–4661; f) S. R. Peurifoy, T. J. Sisto, F. Ng, M. L. Steigerwald, R. Chen, C. Nuckolls, *Chem. Rec.* **2019**, *19*, 1050–1061; g) A. Chuvilin, E. Bichoutskaia, M. C. Gimenez-Lopez, T. W. Chamberlain, G. A. Rance, N. Kuganathan, J. Biskupek, U. Kaiser, A. N. Khlobystov, *Nat. Mater.* **2011**, *10*, 687–692; h) A. Narita, X.-Y. Wang, X. Feng, K. Müllen, *Chem. Soc. Rev.* **2015**, *44*, 6616–6643; i) X. Y. Wang, X. Yao, A. Narita, K. Mullen, *Acc. Chem. Res.* **2019**, *52*, 2491–2505; j) W. Niu, J. Liu, Y. Mai, K. Müllen, X. Feng, *Trends Chem.* **2019**, *1*, 549–558; k) J. Liu, X. Feng, *Angew. Chem. Int. Ed.* **2020**, *59*, 23386–23401; *Angew. Chem.* **2020**, *132*, 23591–23607; l) Z. Chen, A. Narita, K. Müllen, *Adv. Mater.* **2020**, *32*, 2001893.

[2] X.-Y. Wang, A. Narita, K. Müllen, *Nat. Chem. Rev.* **2017**, *2*, 0100.

[3] a) A. Tsuda, A. Osuka, *Science* **2001**, *293*, 79–82; b) S. Ma, J. Gu, C. Lin, Z. Luo, Y. Zhu, J. Wang, *J. Am. Chem. Soc.* **2020**, *142*, 16887–16893.

[4] a) B. Schlicke, A. D. Schlüter, P. Hauser, J. Heinze, *Angew. Chem. Int. Ed. Engl.* **1997**, *36*, 1996–1998; *Angew. Chem.* **1997**, *109*, 2091–2093; b) B. Purushothaman, M. Bruzek, S. R. Parkin, A.-F. Miller, J. E. Anthony, *Angew. Chem. Int. Ed.* **2011**, *50*, 7013–7017; *Angew. Chem.* **2011**, *123*, 7151–7155; c) L. Chen, C. Li, K. Müllen, *J. Mater. Chem. C* **2014**, *2*, 1938–1956; d) J. Liu, B.-W. Li, Y.-Z. Tan, A. Giannakopoulos, C. Sanchez-Sanchez, D. Beljonne, P. Ruffieux, R. Fasel, X. Feng, K. Müllen, *J. Am. Chem. Soc.* **2015**, *137*, 6097–6103; e) K. Ozaki, K. Kawasumi, M. Shibata, H. Ito, K. Itami, *Nat. Commun.* **2015**, *6*, 6251; f) R. Huang, H. Phan, T. S. Herng, P. Hu, W. Zeng, S.-Q. Dong, S. Das, Y. Shen, J. Ding, D. Casanova, J. Wu, *J. Am. Chem. Soc.* **2016**, *138*, 10323–10330; g) W. Zeng, H. Phan, T. S. Herng, T. Y. Gopalakrishna, N. Aratani, Z. Zeng, H. Yamada, J. Ding, J. Wu, *Chem* **2017**, *2*, 81–92; h) W. Fan, T. Winands, N. L. Doltsinis, Y. Li, Z. Wang, *Angew. Chem. Int. Ed.* **2017**, *56*, 15373–15377; *Angew. Chem.* **2017**, *129*, 15575–15579; i) J. Lee, H. Li, A. J. Kalin, T. Yuan, C. Wang, T. Olson, H. Li, L. Fang, *Angew. Chem. Int. Ed.* **2017**, *56*, 13727–13731; *Angew. Chem.* **2017**, *129*, 13915–13919; j) W. Chen, X. Li, G. Long, Y. Li, R. Ganguly, M. Zhang, N. Aratani, H. Yamada, M. Liu, Q. Zhang, *Angew. Chem. Int. Ed.* **2018**, *57*, 13555–13559; *Angew. Chem.* **2018**, *130*, 13743–13747; k) D. Cortizo-Lacalle, J. P. Mora-Fuentes, K. Strutyński, A. Saeki, M. Melle-Franco, A. Mateo-Alonso, *Angew. Chem. Int. Ed.* **2018**, *57*, 703–708; *Angew. Chem.* **2018**, *130*, 711–716; l) D. Cortizo-Lacalle, C. Gozalvez, M. Melle-Franco, A. Mateo-Alonso, *Nanoscale* **2018**, *10*, 11297–11301; m) P. Jin, T. Song, J. Xiao, Q. Zhang, *Asian J. Org. Chem.* **2018**, *7*, 2130–2146; n) U. H. F. Bunz, J. Freudenberg, *Acc. Chem. Res.* **2019**, *52*, 1575–1587; o) W. Chen, F. Yu, Q. Xu, G. Zhou, Q. Zhang, *Adv. Sci.* **2020**, *7*, 1903766; p) G. Liu, C. Xiao, F. Negri, Y. Li, Z. Wang, *Angew.*

Chem. Int. Ed. **2020**, *59*, 2008–2012; *Angew. Chem.* **2020**, *132*, 2024–2028; q) S. Castro-Fernández, C. M. Cruz, I. F. A. Mariz, I. R. Márquez, V. G. Jiménez, L. Palomino-Ruiz, J. M. Cuerva, E. Maçôas, A. G. Campaña, *Angew. Chem. Int. Ed.* **2020**, *59*, 7139–7145; *Angew. Chem.* **2020**, *132*, 7205–7211; r) X. Yang, F. Rominger, M. Mastalerz, *Angew. Chem. Int. Ed.* **2021**, *60*, 7941–7946; *Angew. Chem.* **2021**, *133*, 8020–8025; s) F. Chen, W. Gu, A. Saeki, M. Melle-Franco, A. Mateo-Alonso, *Org. Lett.* **2020**, *22*, 3706–3711; t) R. K. Dubey, M. Melle-Franco, A. Mateo-Alonso, *J. Am. Chem. Soc.* **2021**, *143*, 6593–6600.

[5] a) Y. Zhong, M. T. Trinh, R. Chen, G. E. Purdum, P. P. Khlyabich, M. Sezen, S. Oh, H. Zhu, B. Fowler, B. Zhang, W. Wang, C.-Y. Nam, M. Y. Sfeir, C. T. Black, M. L. Steigerwald, Y.-L. Loo, F. Ng, X. Y. Zhu, C. Nuckolls, *Nat. Commun.* **2015**, *6*, 8242; b) Y. Zhong, T. J. Sisto, B. Zhang, K. Miyata, X. Y. Zhu, M. L. Steigerwald, F. Ng, C. Nuckolls, *J. Am. Chem. Soc.* **2017**, *139*, 5644–5647; c) T. J. Sisto, Y. Zhong, B. Zhang, M. T. Trinh, K. Miyata, X. Zhong, X. Y. Zhu, M. L. Steigerwald, F. Ng, C. Nuckolls, *J. Am. Chem. Soc.* **2017**, *139*, 5648–5651.

[6] a) L. Đorđević, F. Arcudi, M. Cacioppo, M. Prato, *Nat. Nanotechnol.* **2022**, *17*, 112–130; b) P. Reineck, A. Francis, A. Orth, D. W. M. Lau, R. D. V. Nixon-Luke, I. D. Rastogi, W. A. W. Razali, N. M. Cordina, L. M. Parker, V. K. A. Sreenivasan, L. J. Brown, B. C. Gibson, *Adv. Opt. Mater.* **2016**, *4*, 1549–1557; c) P. Reineck, M. Torelli, *Mat. Matters* **2019**, *14*, 57–61.

[7] J. Hu, D. Zhang, F. W. Harris, *J. Org. Chem.* **2005**, *70*, 707–708.

[8] M. Daigle, D. Miao, A. Lucotti, M. Tommasini, J.-F. Morin, *Angew. Chem. Int. Ed.* **2017**, *56*, 6213–6217; *Angew. Chem.* **2017**, *129*, 6309–6313.

[9] E. Clar, *The Aromatic Sextet*, Wiley, London, **1972**.

[10] Y. Chen, C. Lin, Z. Luo, Z. Yin, H. Shi, Y. Zhu, J. Wang, *Angew. Chem. Int. Ed.* **2021**, *60*, 7796–7801; *Angew. Chem.* **2021**, *133*, 7875–7880.

[11] S. More, R. Bhosale, S. Choudhary, A. Mateo-Alonso, *Org. Lett.* **2012**, *14*, 4170–4173.

[12] T. Ren, X. Shen, L. Han, L. Bai, H. Zhao, Y. Wu, H. Wang, X. Ba, *ChemistrySelect* **2016**, *1*, 267–271.

[13] a) X. Guo, Z. Yuan, Y. Zhu, Z. Li, R. Huang, Z. Xia, W. Zhang, Y. Li, J. Wang, *Angew. Chem. Int. Ed.* **2019**, *58*, 16966–16972; *Angew. Chem.* **2019**, *131*, 17122–17128; b) Y. Zhu, Z. Xia, Z. Cai, Z. Yuan, N. Jiang, T. Li, Y. Wang, X. Guo, Z. Li, S. Ma, D. Zhong, Y. Li, J. Wang, *J. Am. Chem. Soc.* **2018**, *140*, 4222–4226; c) Y.-Z. Tan, B. Yang, K. Parvez, A. Narita, S. Osella, D. Beljonne, X. Feng, K. Müllen, *Nat. Commun.* **2013**, *4*, 2646; d) Y. Zhu, X. Guo, Y. Li, J. Wang, *J. Am. Chem. Soc.* **2019**, *141*, 5511–5517; e) X. Yan, X. Cui, L.-S. Li, *J. Am. Chem. Soc.* **2010**, *132*, 5944–5945; f) Y. Wang, Z. Yin, Y. Zhu, J. Gu, Y. Li, J. Wang, *Angew. Chem. Int. Ed.* **2019**, *58*, 587–591; *Angew. Chem.* **2019**, *131*, 597–601.

[14] a) F. Arcudi, L. Đorđević, M. Prato, *Acc. Chem. Res.* **2019**, *52*, 2070–2079; b) Y. Yan, J. Chen, N. Li, J. Tian, K. Li, J. Jiang, J. Liu, Q. Tian, P. Chen, *ACS Nano* **2018**, *12*, 3523–3532.

[15] R. K. Dubey, M. Melle-Franco, A. Mateo-Alonso, *J. Am. Chem. Soc.* **2022**, *144*, 2765–2774.

Manuscript received: April 5, 2022
Accepted manuscript online: April 25, 2022